JACS
JOURNAL OF THE AMERICAN CHEMICAL SOCIETY

Communication

pubs.acs.org/JACS

Solution Synthesis and Reactivity of Colloidal Fe_2GeS_4: A Potential Candidate for Earth Abundant, Nanostructured Photovoltaics

Sarah J. Fredrick and Amy L. Prieto*

Department of Chemistry, Colorado State University, Fort Collins, Colorado 80523, United States

Supporting Information

ABSTRACT: Iron chalcogenides, in particular iron pyrite, have great potential to be useful materials for cost-effective thin film photovoltaics. However, the performance of pyrite as an absorber material in photovoltaic devices has fallen far short of the theoretical efficiency. A potential cause of this may be the instability of the pyrite phase. An alternate class of iron chalcogenides, Fe_2MS_4 (M = Ge, Si) has been proposed as a possible alternative to pyrite, yet has only been studied for interesting magnetic properties. Herein, we report the first solution synthesis of colloidal Fe_2GeS_4 and report the optical properties, reactivity, and potential for use as a photovoltaic material.

In the race to find alternatives to carbon-based fuels, thin film solar cells composed of cheap, earth abundant absorber materials are attractive because they could be economically competitive. One material receiving renewed interest is pyrite, FeS_2 because of its abundance and low cost, large absorption coefficient ($\sim 10^5$ cm^{-1}) and useful band gap ($\sim$0.9 eV).[1,2] However, the reported photovoltaic performance has been quite poor regardless of the synthetic methods or measurements used. The highest reported power conversion efficiency of 3% (compared to the theoretical efficiency of 20%), reported in 1993, has been attributed to very low photovoltages.[3] Various theories have been proposed seeking to explain the disparity between the theoretically predicted performance and the experimentally measured properties including bulk and surface defects,[4−7] sulfur deficiencies,[8] small cores of metallic iron,[9] and domains of amorphous iron sulfide impurity phases with very small band gaps.[10] Although robust syntheses of pyrite nanostructures and thin films have been demonstrated, details of the photovoltaic properties of many of the recently reported samples are largely absent.[6,9,11−16]

Of the various proposed hypotheses for the poor performance observed for pyrite, Yu et al. suggest that the primary hindrance to optimal PV properties for pyrite is the presence of sulfur deficient phases that are more thermodynamically stable than stoichiometric FeS_2.[10] They propose an alternative class of iron chalcogenide photovoltaic materials: Fe_2MS_4 (M = Ge, Si), that could have the same attractive properties as pyrite, but with significantly better phase stability with respect to the decomposition into binary phases. These compounds are predicted to have high absorption coefficients ($>10^5$ cm^{-1}) and band gaps that are larger than those of pyrite (1.40 and 1.55 eV for the Ge and Si compounds, respectively), ideal for solar absorption. These compounds have been well characterized structurally as well as magnetically, but we have no knowledge of reports of either of these materials being evaluated for use in solar cells.

Nanocrystalline solar cell materials are of interest due to the advantage of low temperature processing and the potential to reduce the cost of fabrication.[17] Recent reports have demonstrated nanocrystalline solar cells reaching efficiencies up to 7%,[18] demonstrating the great potential for commercial use. The first step for the incorporation of nanocrystals of new materials into PV devices is a well-developed synthesis of the nanocrystal building blocks. Herein, we report a solution synthesis of colloidal Fe_2GeS_4 nanocrystals for a potential use in solar cells, with particular attention paid to the stability of these particles in air.

Single crystal samples of Fe_2GeS_4 have been made by conventional solid-state methods, and have been structurally characterized.[19−21] This compound adopts an olivine structure with space group *Pnma*. To our knowledge, a solution synthesis has never been reported. Additionally, the optical and photophysical properties have only been discussed in the aforementioned theory paper by Yu and co-workers, but have not been demonstrated experimentally.

Colloidal nanostructures of Fe_2GeS_4 were synthesized by the following method. Approximately 63 mg of $FeCl_2$, 220 mg of GeI_4, 2.0 g of hexadecylamine (HDA) and 2.0 mL of octadecene (ODE) were heated to 320 °C. During the heating process, a solution containing 1.0 mL of hexamethyldisilazane (HMDS), 0.45 mL of hexamethyldisilathiane ($(TMS)_2S$), and 1.0 mL of ODE was injected into the solution at 120 °C. The reaction was left at 320 °C for 24 h (see Supporting Information (SI) for experimental details and analysis of the effect of reaction growth time on phase purity and particle size). The product was washed several times using a combination of acetone and hexanes to remove unreacted starting material. The final product was suspended in either hexanes or toluene. The colloidal suspension is light brown in color and is stable, as determined by the observation that the nanocrystals stay suspended in solution for weeks without agglomeration if stored in a nonpolar solvent in an oxygen-free environment.

The reaction conditions were chosen based upon empirical evidence and previous literature reports on similar materials. Hexadecylamine was used because of its relatively high purity (98% versus the 70% purity of oleylamine which is typically used in high temperature nanoparticle syntheses)[22] and high boiling point (330 °C). Germanium(IV) iodide was chosen as the Ge

Received: August 11, 2013
Published: November 7, 2013

   dx.doi.org/10.1021/ja408333y | *J. Am. Chem. Soc.* 2013, 135, 18256−18259

precursor because of its higher temperature stability as compared to germanium(IV) chloride. When reactions were performed with $GeCl_4$, the product was black, not the brown color indicative of the desired product, and a large amount of white residue (presumably unreacted $GeCl_4$) was present inside the condenser column, likely because of the volatility of the precursor at these reaction temperatures.

The reaction temperature of 320 °C was found to be critical. An example of the product formed from a reaction at a lower temperature (250 °C) is shown in Figure S1. None of the desired product is made at this temperature. There are several crystalline peaks that cannot be definitively identified and do not correspond to likely binary phases (e.g., iron and germanium sulfides). Hexamethyldisilazane has been used in a variety of germanium chalcogenide syntheses, including some ternary compounds,[23,24] and although its mechanism of action in these reactions is not known, it is an important reactant in these syntheses. Reactions without HMDS produced a mixture of the desired product, GeS and FeS (Figure S2). It was also found that the $(TMS)_2S$ precursor was vital to obtain the ternary compound. When sulfur powder was used as the sulfur source, the only phases detected via X-ray diffraction are iron sulfides, regardless of reaction temperature or time. An excess of Ge is also required to obtain a phase-pure product. The stoichiometric ratio of 2:1:4 of Fe:Ge:S was attempted with many reaction conditions and always produced a mixture of Fe_2GeS_4 and FeS. However, when a 2:1.5:4 ratio was used, the desired product was formed (see Figures S3 and S4 for details). X-ray diffraction data of aliquots at various reaction times shows that the desired product begins to form after only 1 h at 320 °C. However, the nanocrystals do not suspend at these short times. Additionally, there is an extra peak at shorter times that is likely an iron sulfide phase. This phase is not present after 24 h. A long reaction time gives a phase-pure colloidal suspension in which the particles do not precipitate out over time. Finally, these samples appear to be relatively stable under inert conditions. Nanocrystals heated under N_2 remain phase pure and fairly crystalline up to 200 °C, as evidenced by XRD showing crystalline Fe_2GeS_4 without the presence of other crystalline phases (Figure S5). All of the following data is for a reaction growth time of 24 h.

X-ray powder diffraction data (Figure 1) shows only the presence of Fe_2GeS_4 with no additional peaks that would indicate the presence of crystalline impurity phases. TEM analysis was performed to determine particle size and morphology (Figure 2).

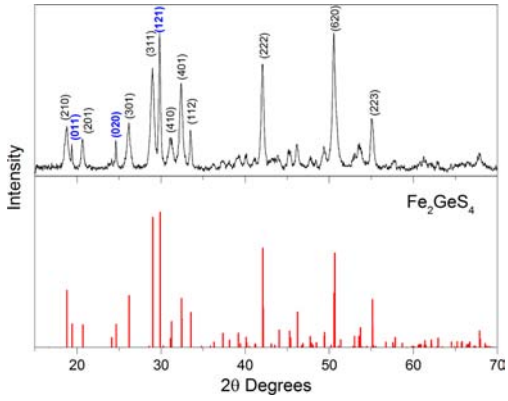

Figure 1. Powder X-ray diffraction of the Fe_2GeS_4 nanocrystals (top). Diffraction pattern simulated using Crystal Maker software (bottom). The original crystal structure data was obtained from ref 21. Well-resolved peaks are labeled with (*hkl*) values and particularly narrow peaks are in blue.

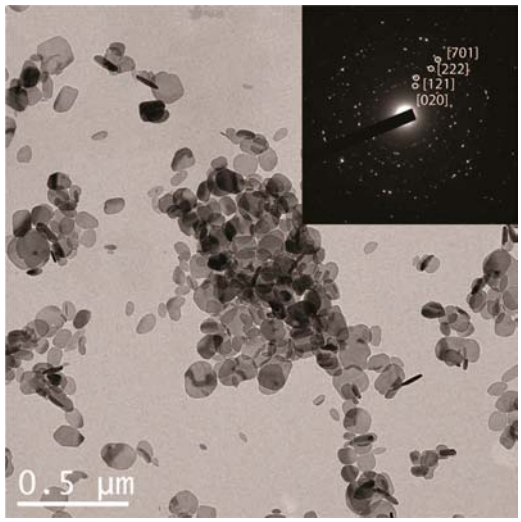

Figure 2. Low resolution TEM image of Fe_2GeS_4 nanocrystals after a 24 h growth time. (Inset) Selected area electron diffraction with four representative spots indexed.

The product is composed of plate-like structures of varying size and shape, with a size distribution of 75.9 ± 30.9 nm. The sizes were determined by measuring >100 particles and calculating an average and standard deviation. Particles that were oblong in shape were measured along both the long and short dimensions, and those values were then averaged. A high resolution TEM image showing clear lattice fringes with a corresponding FFT indexed to Fe_2GeS_4 is shown in Figure S6.

Due to the plate-like appearance of the nanocrystals, a more detailed analysis of the X-ray diffraction data was performed in an effort to identify the crystallographic directions of preferential growth. The full width at half-maximum (fwhm) was measured for well-resolved peaks (all peaks labeled with *hkl* values in Figure 1) and the (011), (020) and (121) peaks were found to be significantly more narrow than the rest. There was not, however, a clear candidate for the orthogonal plane (as indicated by a significantly broader peak). The authors propose that the rapid growth in these three planes may be due to the fact that they contain only Fe and S atoms. Experimentally, we noticed that the reactivity of germanium with sulfur was relatively low compared to that of iron with sulfur (as evidenced by the need for an excess of germanium, and the preference for iron sulfide phases to form under different reaction conditions). It may be possible that planes containing germanium have slower growth rates, leading to the interesting geometry of the nanocrystals.

Selected area electron diffraction was performed to further corroborate the observed preferential growth along certain crystallographic directions. If all of the particles were lying flat, one should be able to determine which crystallographic directions corresponded to the 'thin' axes of the planes. We were not successful obtaining samples where all of the plates lay flat. As can be seen in Figure 2, the majority of the nanocrystals are lying flat, as plates, with the broad side in line with the TEM grid. However, some plates seem to be oriented completely perpendicular to the grid (see Figure S7 for an additional example). From this very small sample size, we estimate the plate thicknesses to be on the order of 7 nm, although there are not

dx.doi.org/10.1021/ja408333y | *J. Am. Chem. Soc.* 2013, 135, 18256−18259

enough of these in the images we took to determine any reasonable statistics.

One of the advantages of using nanocrystals to make solar cells is the potential for fabricating thin films on the benchtop via processes such as dip coating or drop casting. Thus, air stability is a desired property although certainly not a requirement. We performed X-ray photoelectron spectroscopy experiments to determine the initial bonding environments of Fe, Ge and S in the as-made samples, and also to monitor potential changes over time. Four identical experiments were performed: one initial sample was analyzed with as little oxygen exposure as possible (details in SI). The same sample was left in air for 2, 12, and 24 h and analyzed to monitor changes upon exposure to air. The results were quite dramatic.

It is well established in the literature that the Fe XPS can be convoluted by the presence of multiple oxidation states, local bonding environments, and surface states.[25−27] In particular, different iron species, especially Fe(III) and various iron oxides that can be formed upon exposure to air, will overlap. Furthermore, the high percentage of surface states present in these high surface area materials will add an additional degree of complexity. The authors do not seek to definitively identify all of the species present in the Fe_2GeS_4 samples, but rather to identify general trends that may be indications of inherent properties and stability. Figure 3 shows the Fe 2p XPS spectra for all air exposure

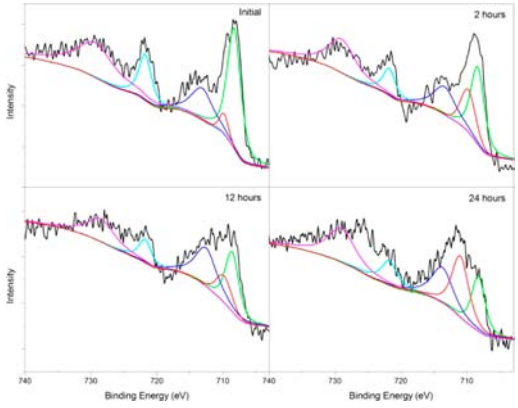

Figure 3. X-ray photoelectron spectroscopy of the Fe 2p energy range for four different times of air exposure: (clockwise from top left) initial, 2, 12, and 24 h. Black traces are raw data and colored traces are fitted peaks.

times. The black traces are the raw data, while the colored traces are the fits. A typical Fe(II) sulfide spectrum with no Fe(III), surface states, or multiplet impurities would only contain the green (708.3 eV) and light blue (721.8 eV) peaks.[28,29] It is clear that even in the initial scan, a variety of Fe binding environments are present. We suspect that this is due to rapid oxidation in the several seconds of air exposure during sample transfer to the XPS chamber rather than an inherent mixture of Fe binding environments (which would not be expected from the structure). What becomes clear over time is the continued oxidation from Fe(II) to Fe(III) that occurs in air (dark blue and magenta), resulting in an increase in the area under the curve for Fe(III) as compared to the Fe(II). The red trace is another species that increases over time. This fit is assigned to FeO, which is consistent with the literature.[29,30] It is clear that the Fe species oxidize significantly upon exposure to air.

The Ge XPS spectra provided a much more straightforward picture of the chemical changes occurring in the sample (Figure 4). Initially, the Ge exists almost entirely in a binding energy range that is typical for germanium(IV) sulfide (reported to be

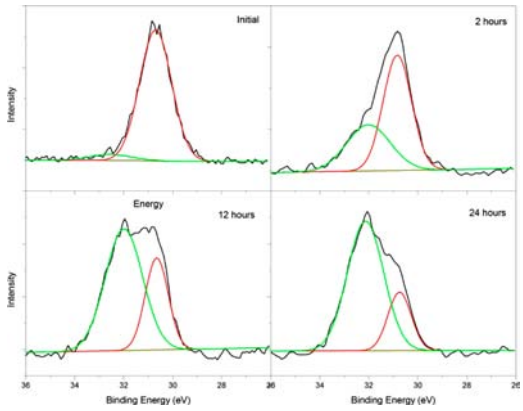

Figure 4. X-ray photoelectron spectroscopy data of the Ge 3d energy range for four different times of air exposure: (clockwise from top left) initial, 2, 12, and 24 h. Black traces are raw data and colored traces are fitted peaks.

30.4 eV)[31] shown with the red fit. The data exhibit a small shoulder, indicating the presence of a higher energy binding environment (green trace), more typical of Ge(IV) oxide (32.4 eV).[31] This progression continues, and after only 12 h, there is more GeO_2 than GeS_2 (a quantitative comparison as a function of time is shown in the SI Table 1). The changes in the sulfur binding environment are minimal and are likely attributed to small amounts of polysulfides forming (Figure S8),[32] which is consistent with the general oxidation of the compound that occurs upon exposure to air. Although these changes are rapid and apparent in XPS, the oxides that form are amorphous and do not appear in the diffraction pattern.

High resolution TEM images confirm the presence of an amorphous layer on the particles, approximately 10 nm in thickness, that forms upon exposure to air (see Figure S9). Lattice fringes are observed in the core of the particle, even after significant surface oxidation.

To determine the potential for future use in photovoltaics, UV−Vis spectroscopy and photoelectrochemical tests were performed on the nanocrystals. The UV−Vis spectrum exhibits a very gradual onset of absorption (Figure S10) which could be due to the challenges often associated with the electronic transitions present for octahedral Fe(II), the presence of amorphous phases on the surface (particularly amorphous iron oxides, which exhibit similar broad absorption), or the presence of a range of other surface states. Hence, we are not able to estimate a band gap. However, it is clear that the material does absorb in the visible region.

Thin films of the nanoparticles were made so that photoelectrochemistry could be used to measure photocurrent as a function of potential applied to the film. Photocurrent was measured in a three electrode photoelectrochemical cell (see SI for details). This preliminary data shows that photocurrent is indeed generated at modest potentials under illumination with green light, and that the photocurrent is p-type, as expected (Figures S11 and S12). The current density is small, but it should be noted that the film thickness and ligand capping were not optimized, and although these samples were tested in a solution that had been thoroughly degassed with nitrogen, we cannot be sure that surface oxidation did not impede good transport within the films. Further optimization of the PEC setup including

dx.doi.org/10.1021/ja408333y | J. Am. Chem. Soc. 2013, 135, 18256−18259

rigorous air-free measurements and improved thin film fabrication are required for enhanced performance.

The observed oxidation in air is not ideal, and may hint at poor surface capping. In an effort to demonstrate the potential for future surface modification as a route toward enhanced stability, a ligand exchange was performed to cap the surface of the particles with S^{2-} ligands[33] to ensure proper sulfide termination. We found a complete ligand exchange occurred, removing all HDA capping ligands as determined by IR spectroscopy (Figure S13). Furthermore, preliminary XPS data suggests that this simple ligand exchange slows the oxidation of the germanium species significantly (Figure S14 and SI Table 1). There are a variety of other capping agents for nanocrystals that have been reported in recent literature.[18,34−36] Future work utilizing these capping agents is an advantageous route for mitigating the surface oxidation problems and enhancing PV properties. Studies are currently underway to explore surface treatments for Fe_2GeS_4 nanocrystals.

We have shown that phase pure Fe_2GeS_4 colliodal nanostructures can be synthesized from solution. The resulting nanostructures appear to be plate-like and remain suspended in solution for extended periods of time. Preliminary data suggest air stability can be achieved by post synthetic surface treatments. The particles are p-type and readily produce photocurrent, indicating their potential for future use in solar cells. To our knowledge, this is the first report of the synthesis of colloidal, crystalline Fe_2GeS_4 and the first report of photocurrent obtained at modest potentials for this material.

■ ASSOCIATED CONTENT

Supporting Information

Further data and analysis including experimental details, XRD, TEM, XPS, UV−Vis, FTIR and photoelectrochemistry. This material is available free of charge via the Internet at http://pubs.acs.org.

■ AUTHOR INFORMATION

Corresponding Author

Amy.Prieto@colostate.edu

Notes

The authors declare no competing financial interest.

■ ACKNOWLEDGMENTS

A.L.P. gratefully acknowledges support from the Research Corporation for Science Advancement and S.J.F. gratefully acknowledges the NSF GRF program, DGE-0822211. We thank the Microscope Imaging Network at CSU (low resolution TEM), and the University of Wyoming School of Energy Resources (high resolution TEM).

■ REFERENCES

(1) Wadia, C.; Alivisatos, A. P.; Kammen, D. M. *Environ. Sci. Technol.* **2009**, *43*, 2072.

(2) Ennaoui, A.; Tributsch, H. *Sol. Cells* **1984**, *13*, 197.

(3) Ennaoui, A.; Fiechter, S.; Pettenkofer, C.; Alonsovante, N.; Buker, K.; Bronold, M.; Hopfner, C.; Tributsch, H. *Sol. Energy Mater. Sol. Cells* **1993**, *29*, 289.

(4) Bronold, M.; Pettenkofer, C.; Jaegermann, W. *J. Appl. Phys.* **1994**, *76*, 5800.

(5) Bronold, M.; Tomm, Y.; Jaegermann, W. *Surf. Sci.* **1994**, *314*, L931.

(6) Berry, N.; Cheng, M.; Perkins, C. L.; Limpinsel, M.; Hemminger, J. C.; Law, M. *Adv. Energy Mater.* **2012**, *2*, 1124.

(7) Caban-Acevedo, M.; Liang, D.; Chew, K. S.; DeGrave, J. P.; Kaiser, N. S.; Jin, S. *ACS Nano* **2013**, *7*, 1731.

(8) Birkholz, M.; Fiechter, S.; Hartmann, A.; Tributsch, H. *Phys. Rev. B* **1991**, *43*, 11926.

(9) Zhang, X.; Manno, M.; Baruth, A.; Johnson, M.; Aydil, E. S.; Leighton, C. *ACS Nano* **2013**, *7*, 2781.

(10) Yu, L.; Lany, S.; Kykyneshi, R.; Jieratum, V.; Ravichandran, R.; Pelatt, B.; Altschul, E.; Platt, H. A. S.; Wager, J. F.; Keszler, D. A.; Zunger, A. *Adv. Energy Mater.* **2011**, *1*, 748.

(11) Puthussery, J.; Seefeld, S.; Berry, N.; Gibbs, M.; Law, M. *J. Am. Chem. Soc.* **2010**, *133*, 716.

(12) Seefeld, S.; Limpinsel, M.; Liu, Y.; Farhi, N.; Weber, A.; Zhang, Y.; Berry, N.; Kwon, Y. J.; Perkins, C. L.; Hemminger, J. C.; Wu, R.; Law, M. *J. Am. Chem. Soc.* **2013**, *135*, 4412.

(13) Bai, Y.; Yeom, J.; Yang, M.; Cha, S.-H.; Sun, K.; Kotov, N. A. *J. Phys. Chem. C* **2013**, *117*, 2567.

(14) Gong, M.; Kirkeminde, A.; Ren, S. *Sci. Rep.* **2013**, *3*, 2092.

(15) MacPherson, H. A.; Stoldt, C. R. *ACS Nano* **2012**, *6*, 8940.

(16) Kirkeminde, A.; Ruzicka, B. A.; Wang, R.; Puna, S.; Zhao, H.; Ren, S. *ACS Appl. Mater. Interfaces* **2012**, *4*, 1174.

(17) Habas, S. E.; Platt, H. A. S.; van Hest, M. F. A. M.; Ginley, D. S. *Chem. Rev.* **2010**, *110*, 6571.

(18) Ip, A. H.; Thon, S. M.; Hoogland, S.; Voznyy, O.; Zhitomirsky, D.; Debnath, R.; Levina, L.; Rollny, L. R.; Carey, G. H.; Fischer, A.; Kemp, K. W.; Kramer, I. J.; Ning, Z.; Labelle, A. J.; Chou, K. W.; Amassian, A.; Sargent, E. H. *Nat. Nanotechnol.* **2012**, *7*, 577.

(19) Junod, A.; Wang, K. Q.; Triscone, G.; Lamarche, G. *J. Magn. Magn. Mater.* **1995**, *146*, 21.

(20) Ohgushi, K.; Ueda, Y. *Phys. Rev. Lett.* **2005**, 95.

(21) Vincent, H.; Bertaut, E. F.; Baur, W. H.; Shannon, R. D. *Acta Crystallogr., Sect. B: Struct. Sci.* **1976**, *32*, 1749.

(22) Mourdikoudis, S.; Liz-Marzán, L. M. *Chem. Mater.* **2013**, *25*, 1465.

(23) Antunez, P. D.; Buckley, J. J.; Brutchey, R. L. *Nanoscale* **2011**, *3*, 2399.

(24) Vaughn, D. D.; Patel, R. J.; Hickner, M. A.; Schaak, R. E. *J. Am. Chem. Soc.* **2010**, *132*, 15170.

(25) Biesinger, M. C.; Payne, B. P.; Grosvenor, A. P.; Lau, L. W. M.; Gerson, A. R.; Smart, R. S. C. *Appl. Surf. Sci.* **2011**, *257*, 2717.

(26) Mullet, M.; Boursiquot, S.; Abdelmoula, M.; Genin, J.-M.; Ehrhardt, J.-J. *Geochim. Cosmochim. Acta* **2002**, *66*, 829.

(27) Nesbitt, H. W.; Scaini, M.; Hochst, H.; Bancroft, G. M.; Schaufuss, A. G.; Szargan, R. *Am. Mineral.* **2000**, *85*, 850.

(28) Panzner, G.; Egert, B. *Surf. Sci.* **1984**, *144*, 651.

(29) Brion, D. *Appl. Surf. Sci.* **1980**, *5*, 133.

(30) Hawn, D. D.; DeKoven, B. M. *Surf. Interface Anal.* **1987**, *10*, 63.

(31) Hollinger, G.; Kumurdjian, P.; Mackowski, J. M.; Pertosa, P.; Porte, L.; Duc, T. M. *J. Electron Spectrosc. Relat. Phenom.* **1974**, *5*, 237.

(32) Pratt, A. R.; Muir, I. J.; Nesbitt, H. W. *Geochim. Cosmochim. Acta* **1994**, *58*, 827.

(33) Nag, A.; Kovalenko, M. V.; Lee, J. S.; Liu, W. Y.; Spokoyny, B.; Talapin, D. V. *J. Am. Chem. Soc.* **2011**, *133*, 10612.

(34) Kovalenko, M. V.; Scheele, M.; Talapin, D. V. *Science* **2009**, *324*, 1417.

(35) Luther, J. M.; Law, M.; Song, Q.; Perkins, C. L.; Beard, M. C.; Nozik, A. J. *ACS Nano* **2008**, *2*, 271.

(36) Fafarman, A. T.; Koh, W.-k.; Diroll, B. T.; Kim, D. K.; Ko, D.-K.; Oh, S. J.; Ye, X.; Doan-Nguyen, V.; Crump, M. R.; Reifsnyder, D. C.; Murray, C. B.; Kagan, C. R. *J. Am. Chem. Soc.* **2011**, *133*, 15753.